The use of Josephson junctions in constructing qubits with long decoherence times

Topic: Quantum entanglement and Quantum information

Andrea Kouta Dagnino

PI: F7907843

A Report submitted as the examined component

of the Project Module SXP390

The Open University

Date of submission: September 13, 2022

ABSTRACT

Superconductivity is a low-temperature quantum phenomenon in which electrons condense into doublets known as Cooper pairs, whose wave-functions are characterised by the same quantum phase. This macroscopic quantum coherence effect has in the last two decades opened the way for the realisation of Superconducting Qubits (SQubits). In particular, three qubit designs have been proposed which exploit the charge, flux and phase quantum numbers of Josephson junctions to store information.

In this review we survey the theory of superconductivity and the closely-related Josephson effect whereby Cooper pairs coherently tunnel through a thin insulating barrier between two superconductors, leading to current flow in absence of a bias voltage. We review the properties of charge, flux and phase SQubits, discussing their individual strengths and drawbacks for integrability in quantum computers.

We then review the theory of quantum decoherence, where information stored in a system gets lost to its environment via relaxation or decay, and explain why it poses a serious obstacle to implementing SQubits in large-scale quantum circuits. We focus in particular on charge noise, flux noise and dielectric losses as the dominant decoherence mechanisms. Proposed theoretical models for noise sources and suggested mitigation mechanisms are discussed at length, in conjunction with on-going experimental progress in probing and suppressing these effects. These include operating qubits at optimal bias points, treating the qubits with UV illumination or exposure to NH_3, and using dielectrics with lower loss-tangents.

Decoherence has so far limited qubit life-times to sub-millisecond times, but recent developments in material sciences are showing great promise in breaking through the millisecond barrier. We review these advances and discuss their implications on the future of superconducting quantum computation. Finally, a time-frame for upcoming milestones in mitigating decoherence in SQubits is suggested, highlighting directions for future research.

Word count: 299

Contents

Titlepage 1

Abstract 2

List of Figures 4

1 ***Introduction*** 6
- 1.1 Background . . . 6
- 1.2 Objectives . . . 7
- 1.3 Scopes of the work . . . 7
- 1.4 Search methodology . . . 7

2 ***Superconductivity and Josephson junctions*** 8
- 2.1 The BCS theory of superconductivity . . . 8
- 2.2 The Josephson effect . . . 9

3 ***SQubits: charge, phase and flux*** 11
- 3.1 Charge qubits . . . 11
- 3.2 Flux qubits . . . 12
- 3.3 Phase qubits . . . 13

4 ***Decoherence in SQubits: sources and mitigation*** 14
- 4.1 Theory of decoherence in qubits . . . 14
- 4.2 Charge noise and optimal bias points . . . 15
- 4.3 Flux noise . . . 16
- 4.4 Dielectric losses . . . 19

5 ***Discussions and Outlook*** 22
- 5.1 Approaching millisecond coherence . . . 22
- 5.2 Directions for future research . . . 23
- 5.3 Milestones and predicted time-frame . . . 24

6 Conclusions **26**
6.1 Summary 26
6.2 Achievement of project objectives 26

References **29**

List of Figures

2.1 Two possible electron-phonon interactions 8
2.2 (a) Tunnelling in superconductors, image taken from Girvin (2014) and (b) tunnelling in normal metals, image taken from Langford (2013). 10

3.1 Set-up of the Cooper box. Image taken from Bouchiat *et al.* (1998) 11
3.2 Set up of the flux qubit (left) and the resulting potential well (right). Figure adapted from You and Nori (2005). 12
3.3 Set up of the phase qubit (left) and the resulting potential well (right). Figure adapted from You and Nori (2005). 13

4.1 The first three energy levels of a charge qubit as E_J/E_C is increased. The optimal bias points in (a) are marked in dashed lines. Figure taken from Koch J. *et al.* (2007). 15
4.2 The relaxation rate Γ_1, echo pure dephasing rate $\Gamma^g_{\varphi E}$ and free induction decay pure dephasing rate $\Gamma^g_{\varphi F}$ for sample 1 (left) and sample 2 (right) as a function of the flux bias n_ϕ. A linear best fit for the dephasing rates are shown in red. Figure adapted from Yoshihara *et al.* (2006). 16
4.3 (a) Flux noise power spectrum exhibiting a $1/f$ behaviour (data in dots, fit in dashed lines). Figure taken from Bialczak *et al.* (2007), (b) Temperature dependence of the quasistatic flux threading an Al SQUID and a Nb SQUID. Figure taken from Sendelbach *et al.* (2008). 17
4.4 Left: Temperature-dependence of the flux threading a Nb SQUID at different applied fields. Right: the total flux change as a function of the applied field. Figures taken from Sendelbach *et al.* (2008). 17
4.5 The difference in the flux noise spectrum for NH_3 exposed SQUIDs (green, top panel) and UV exposed SQUIDs (purple, bottom panel), versus at conventional conditions (red). Figure taken from Kumar *et al.* (2016). 18

4.6 (a) Top: spectroscopy of a JJ showing spurious resonances at bias points shown with dashed lines. Bottom: $|1\rangle$ occupation probability over time as a function of the bias current. (b) Rabi oscillations (offset) at different bias currents labelled by a, b, c, d, e, f indicated with arrows in (a). Both figures taken from Simmonds *et al.* (2004). 19
4.7 (a) Qubit spectroscopy with solid (dashed) arrow indicating on(off)-resonance. (b) Probability of tunnelling as a function of Rabi pulse time at off-resonant (dashed line) and resonant (solid line) bias currents. Both figures adapted from Cooper *et al.* (2004). 20
4.8 Left: spectroscopy of phase qubits with junction areas $13\mu m^2$ and $70\mu m^2$. Right: normalised cumulative distribution of the size of the resonance splittings. The solid black line shows the distribution predicted by the charge fluctuation model in the smaller qubit. Figure taken from Martinis *et al.* (2005). 21

5.1 Timeline showing the progress in increasing superconducting qubit lifetimes. Figure taken from Kjaergaard (2020). 23
5.2 IBM's road-map for quantum computation in the near future. Figure adapted from IBM (2022). 24

CHAPTER

ONE

INTRODUCTION

1.1 Background

Quantum computation is a proposed form of computation where information is stored in quantum bits (qubits). Unlike classical bits which are binary in nature, qubits can be in a superposition of two states, thus allowing us to harness quantum effects to perform efficient computation. In the last 20 years, proposals exploiting the phase coherence of superconducting materials to construct qubits have started to garner significant interest. Such SQubits are two level quantum systems engineered by adding Josephson tunnelling junctions to LC circuits (Oliver and Welander, 2013). The result is an anharmonic potential with quantised energy levels of junction charge, flux or phase quantum numbers, which can be tuned to behave as two level systems when cooled to millikelvin temperatures. SQubits have the advantage of straightforward scalability using conventional integrated-circuit manufacturing techniques. Nevertheless, they are highly susceptible to decoherence mechanisms leading to relatively low decoherence lifetimes (You and Nori, 2005). This is a critical flaw as quantum gate operations mandate sufficiently long qubit life-times and QEC codes have error-thresholds that are currently outside of reach (Barends *et al.*, 2014). Unfortunately, the problem of identifying and suppressing decoherence in superconducting quantum bits has proven to be significantly difficult. Current decoherence times are still much lower than the theoretical limits imposed by the materials used, although recent breakthroughs in materials sciences are starting to close this gap (Place *et al.*, 2021). In this paper we review the theory of superconductivity and the Josephson effect, and explain how they can be harnessed to construct qubits. We distinguish between three different families of SQubits, and discuss the decoherence sources that most affect

them. Mitigation mechanisms are explored from both a theoretical and experimental perspective. Finally, a time-line for prospective advances in the field is provided.

1.2 Objectives

The project objectives and relevant module themes are enumerated below:

(1) Provide a general overview of the physics behind superconductivity and the Josephson effect. [Contextualisation theme]

(2) Explain how Josephson junctions can be used to create three families of SQubits. [Contextualisation and Development/Application theme]

(3) Survey the coherence properties of SQubits, describing possible sources of decoherence and how they could be mitigated. [Development/Application theme]

(4) Conclude with a discussion on the possible directions for future research in superconducting quantum computation and the predicted time-scales for these improvements to be implemented. [Detailed analysis theme]

1.3 Scopes of the work

This review focuses on the proposed superconducting single-qubit models and the decoherence mechanisms that most affect them. Thus, we will not concern ourselves with details of read-out mechanisms, qubit coupling, quantum error-correction, circuit components and set-up, and fabrication/manufacturing processes, except in the discussions chapter where we outline future research directions.

1.4 Search methodology

Google scholar, the OU library, and google searches were used to find research papers. Key search words included: SQubits, josephson qubits, SQubits decoherence. Relevant literature was selected by reading through the abstracts and skimming through the results section. The reliability of selected references, especially recent ones which have not been fully peer-reviewed yet, was determined using PROMPT. Most referenced papers were published in Nature, Physical Review Letters, Physical Review B, Reviews of Modern physics which are peer-reviewed, high impact-factor journals and therefore reliable sources of information. Conclusions from published papers, as well as road-maps presented by companies specialising in quantum computation were used to draw inspiration for the discussions and outlook chapter.

CHAPTER

TWO

SUPERCONDUCTIVITY AND JOSEPHSON JUNCTIONS

2.1 The BCS theory of superconductivity

Viewing the crystal lattice of a superconductor as an array of ions coupled by oscillators, then the lattice excitations, known as phonons, consist of oscillations of ions about their equilibrium positions. An electron-phonon interaction can consist of an electron absorbing the energy from a phonon or an electron emitting energy as a phonon (Bruus and Flensberg, 2004, p.64).

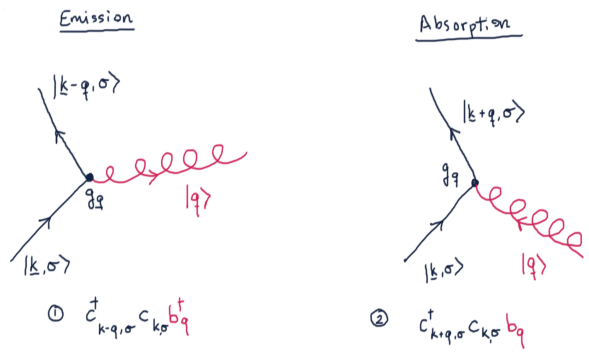

Figure 2.1. Two possible electron-phonon interactions

As an electron moves in the vicinity of (positively charged) ions in the lattice, it will displace them from their equilibrium position due to an attractive Coulomb interaction, thus producing a phonon. As the ions neighbouring the electron get pulled towards it, the electron gets dressed with a net positive charge so that a second electron will be attracted to it

and absorb the phonon it created. Despite being quite naive, this picture is supported by the actual calculations (Girvin and Yang, 2019, pp.593-594) which show that the Coulomb interaction gets screened into an attractive, phonon-exchange-mediated interaction.

This effective interaction leads to the Cooper instability: states a Debye energy within Fermi surface will lower their energy by pairing into opposite spin, opposite momenta pairs (Girvin and Yang, 2019, p.595) known as Cooper pairs. At sufficiently low temperatures, the binding energy of these pairs is large enough to protect them from breaking up implying that Cooper pairs cannot undergo scattering processes like electrons in a normal conductor. When one includes the effective Hamiltonian for these Cooper pairs, the ground state turns out to be analogous to a (coherent) condensate of Cooper pairs as explained in Girvin and Yang (2019, p.610) and Simon (2022, pp.167-171), with the complication that the Cooper pair creation operator is not exactly a bosonic operator. The phase coherence between all the electrons is what leads to several macroscopic, low-temperature quantum effects such as the Josephson effect.

2.2 The Josephson effect

To investigate the Josephson effect we consider two superconductors with a fixed total number $N = N_L + N_R$ of Cooper pairs, separated by a thin tunnelling junction. It is convenient to introduce the Cooper number basis $\{|m\rangle\}$ where $|m\rangle \equiv |N_L - m, N_R + m\rangle$ represents a state where m pairs have been removed from the left superconductor and added to the right superconductor (Girvin, 2014, p.38) relative to some reference state $|0\rangle \equiv |N_L, N_R\rangle$. Due to Andreev reflection (Annett, 2004, p.144), Cooper pairs can tunnel through barriers maintaining their phase coherence as long as the barrier thickness is less than superconducting coherence length. This suggests writing down a tight-binding-like Hamiltonian (Girvin, 2014, pp.39-41)

$$\hat{H} = -\frac{1}{2}E_J \sum_{m=-\infty}^{\infty} \left(|m+1\rangle\langle m| + |m\rangle\langle m+1|\right) \tag{2.2.1}$$

where E_J is some phenomenological energy scale. The current is then given by

$$\hat{I} = i\frac{e}{\hbar}E_J \sum_{m=-\infty}^{\infty} \left(|m+1\rangle\langle m| - |m\rangle\langle m+1|\right) \tag{2.2.2}$$

Following our analogy with the tight-binding approximation we consider the phase basis which is conjugate to the Cooper pair number basis:

$$|\varphi\rangle = \sum_{m=-\infty}^{\infty} e^{i\varphi m}|m\rangle \tag{2.2.3}$$

The phase basis diagonalises the current operator nicely and we find that

$$I = \frac{2e}{\hbar} E_J \sin\varphi \tag{2.2.4}$$

which is the famous DC Josephson relation. A microscopic derivation (Bruus and Flensberg, 2004, pp. 343-346) yields the Ambegaokar-Baratoff formula

$$E_J = \frac{1}{2}\frac{\hbar}{(2e)^2}\frac{1}{R_N}\Delta(T)\tanh\left(\frac{\Delta(T)}{2k_BT}\right) \tag{2.2.5}$$

where R_N is the normal state resistance. We could not derive this result because in our phenomenological description we have omitted the BCS Hamiltonian. The full microscopic derivation includes these terms but nevertheless still assumes that the Cooper pair tunnelling may be expressed as a tunnelling Hamiltonian (a second quantised form of (2.2.1)).

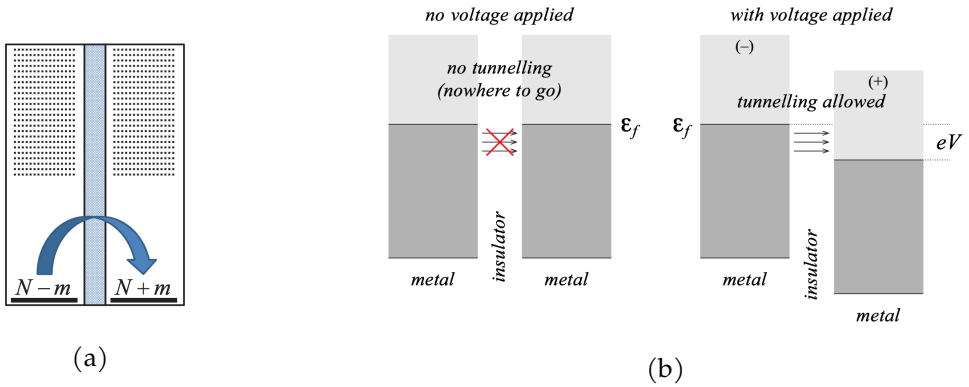

(a) (b)

Figure 2.2. (a) Tunnelling in superconductors, image taken from Girvin (2014) and (b) tunnelling in normal metals, image taken from Langford (2013).

The key difference which allows for Josephson tunnelling is that Cooper pairs are bosonic. Therefore, tunnelling between degenerate states is possible, in contrast to a normal metal where a voltage must be applied to offset the Fermi surfaces and create empty states on one metal for electrons to tunnel into (see fig. 2.2).

CHAPTER

THREE

SQUBITS: CHARGE, PHASE AND FLUX

3.1 Charge qubits

Our treatment of Josephson tunnelling has so far ignored the capacitance developed between the superconductors. Therefore, let's consider a slightly modified set-up introduced by Bouchiat *et al.* (1998) where a small superconducting 'island' is connected to a Cooper pair reservoir forming a parallel-plate capacitor with capacitance C_J. A current is formed in response to a voltage V applied between the reservoir and a gate electrode which is capacitatively coupled to the island by means of a gate capacitance C_g.

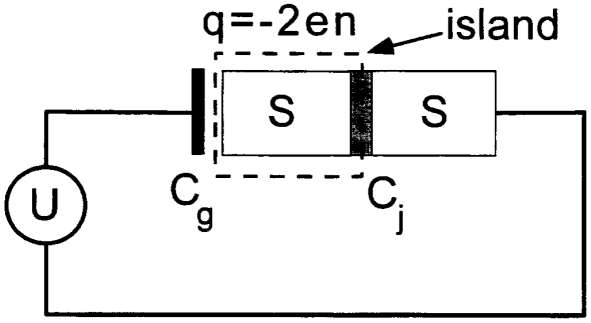

Figure 3.1. Set-up of the Cooper box. Image taken from Bouchiat *et al.* (1998)

The effective Hamiltonian for this system can be written as

$$\hat{H} = E_C \sum_n (\hat{n} - n_g)^2 \left|n\right\rangle \left\langle n\right| - E_J \cos\hat{\varphi},\ E_C = \frac{(2e)^2}{2C_\Sigma}, C_\Sigma = C_g + C_J,\ n_g = \frac{C_g U}{2e} \quad (3.1.1)$$

We consider the "charging regime" $E_J \ll E_C$ where the number operator is the appropriate quantum number. If $E_J = 0$ then we simply get parabolic energy bands crossing at degeneracy points. The importance of the Josephson coupling is to lift this degeneracy and create avoided level crossings which can be used to engineer quantum bits. In particular if $k_B T \ll E_C$ then one can model the system as an effective 2-level system and ignore higher energy bands.

3.2 Flux qubits

Flux qubits are the magnetic analogue of charge qubits in many ways (Girvin, 2014; Devoret and Martinis, 2004). Instead of a gate capacitor, a superconducting transformer consisting of an external current source inductively coupled to a superconducting quantum interference device (SQUID) is used to tune the qubit parameters.

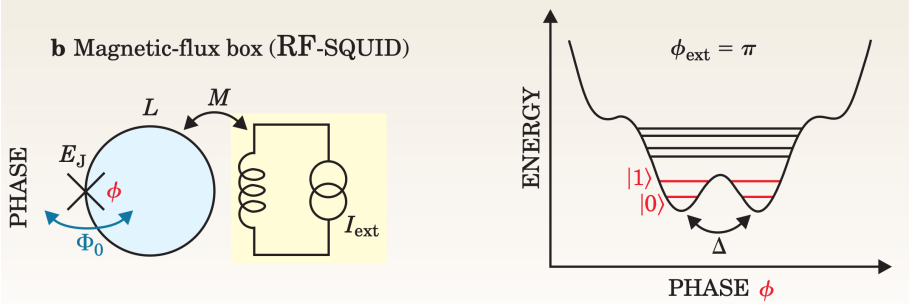

Figure 3.2. Set up of the flux qubit (left) and the resulting potential well (right). Figure adapted from You and Nori (2005).

The flux-qubit is modelled by the following Hamiltonian operated in the phase regime $E_J \gg E_C$

$$\hat{H}_{\text{flux}} = \frac{\hat{Q}^2}{2C} + \underbrace{\frac{\hat{\Phi}^2}{2L} - E_J \cos\left[\frac{2\pi}{\Phi_0}(\hat{\Phi} - \Phi_{\text{ext}})\right]}_{U(\Phi)} \tag{3.2.1}$$

where I_0, C and $E_J = \frac{I_0 \Phi_0}{2\pi}$ are the Josephson junction (JJ) critical current, capacitance and energy respectively, $E_C = \frac{(2e)^2}{2C}$ is the charging energy, L is the SQUID inductance, $\hat{Q}$ and $\hat{\Phi}$ are canonically conjugate charge and flux operators for the qubit, $\Phi_0 = \frac{h}{2e}$ is the magnetic flux quantum and Φ_{ext} is the externally applied flux. We see that the SQUID introduces a non-linear potential $U(\Phi)$ to the circuit (see fig. 3.2) with wells roughly localised at integer flux quanta $n\Phi_0$. When the externally applied flux is set to be $\Phi = (n + \frac{1}{2})\Phi_0$, flux quantisation forces the current around the SQUID to produce an additional half-integer flux $\pm\frac{\Phi_0}{2}$, leading to a total flux of $n\Phi_0$ or $(n+1)\Phi_0$. At some system parameters, $U(\Phi)$ becomes symmetric and the flux states localised at different wells become (nearly) degenerate, allowing for coherent tunnelling. This tunnelling leads to a macroscopic change in

flux which can be read out using an external SQUID (Friedman *et al.*, 2000).

3.3 Phase qubits

The phase qubit is controlled using a bias DC current I_b which is driven across a JJ (Girvin, 2014; Devoret and Martinis, 2004).

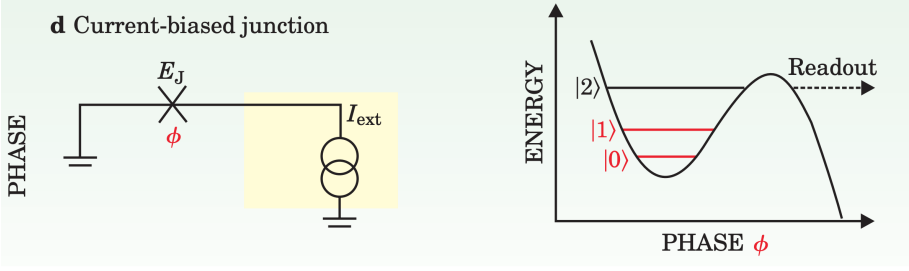

Figure 3.3. Set up of the phase qubit (left) and the resulting potential well (right). Figure adapted from You and Nori (2005).

The potential describing this system is the tilted washboard potential

$$U(\varphi) = -I\varphi_0\varphi - I_0\varphi_0\cos\varphi \tag{3.3.1}$$

where I_0 is the Josephson critical current and φ is the phase across the JJ. This potential produces a number of wells with bound energy states. Unlike charge and flux qubits, phase qubits come with a built-in read-out mechanism (You and Nori, 2005). Indeed, it is not generally possible to significantly decouple the third energy level $|2\rangle$ in a well from the lowest two $|0\rangle, |1\rangle$ which form the phase qubit. Hence one can send microwave pulses to induce $|1\rangle \to |2\rangle$ transitions, so that the system can subsequently tunnel out of the well and be read-out.

CHAPTER

FOUR

DECOHERENCE IN SQUBITS: SOURCES AND MITIGATION

4.1 Theory of decoherence in qubits

Engineering a closed, isolated quantum system would be a completely futile effort because it would make it impossible to implement a read-out mechanism. To allow qubits to be manipulated, one must be able to tune the system's parameters. Unfortunately this tunability allows the environment to couple with the system, leading to decoherence: the loss of information stored in the qubit. Decoherence is driven by interactions between the system and its environment, and can occur either via relaxation/decay or dephasing (Langford, 2013). The former refers to when a qubit in its excited state $|1\rangle$ decays to its ground state $|0\rangle$ by transferring energy to its environment e.g. by spontaneous decay. The qubit can then be made to absorb energy (e.g. from a microwave) and jump back to $|1\rangle$, thus repeating the cycle. This process is known as a Rabi cycle, which forms Rabi oscillations when probing the probability of occupation of $|1\rangle$. Relaxation is characterised by the decay lifetime T_1 corresponding to the inverse decay rate of the excited state. Dephasing on the other hand is a non-dissipative process which does not involve energy exchange. Instead dephasing occurs when a superposition of quantum states loses its phase coherence, and is characterised by a dephasing lifetime T_2 given by

$$\frac{1}{T_2} = \frac{1}{T_1} + \frac{1}{T_\phi} \tag{4.1.1}$$

This quantity receives a contribution from T_1, since relaxation necessary destroys phase coherence, and the pure dephasing lifetime T_ϕ, which describes the dephasing of trans-

verse degrees of freedom $\langle\sigma_x\rangle$, $\langle\sigma_y\rangle$.

Decoherence mechanisms in qubits have been reviewed extensively (Schlosshauer, 2019; Oliver and Welander, 2013). We distinguish between three different sources: charge noise, flux noise and dielectric losses.

4.2 Charge noise and optimal bias points

Variations in the qubit Hamiltonian's parameters lead to fluctuations in the resonant frequency $\omega_{01} = \frac{\Delta E}{\hbar}$. This is especially true for charge qubits where fluctuations in the gate charge n_g can severely affect performance (Nakamura, 2002). Consequently, one would ideally operate the qubit at optimal bias points where the energy splitting ΔE is independent of system parameters. At these points the system is insensitive to fluctuations to first order.

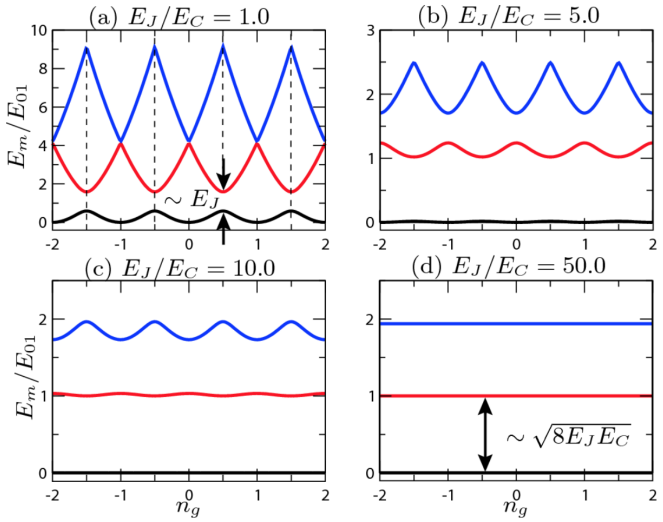

Figure 4.1. The first three energy levels of a charge qubit as E_J/E_C is increased. The optimal bias points in (a) are marked in dashed lines. Figure taken from Koch J. *et al.* (2007).

This observation was first made by Vion *et al.* (2002) who introduced the quantronium qubit, a modified charge qubit driven in the $E_J \approx E_C$ regime. With this ordering of the energy scales, the qubit states don't have a well-defined Cooper charge, making them less sensitive to charge noise. The limitation of this approach is that the qubit can only be operated in a limited region of its configuration space. This led to the invention of the transmon qubit by Koch, J. *et al.* (2007). The authors propose to operate the charge qubit in the strong phase regime $E_J \gg E_C$ where the qubit energy levels are effectively decoupled from the gate charge n_g, thus exponentially suppressing dephasing due to charge noise. The drawback is that the anharmonicity of the system required to form a qubit also decreases with

E_C/E_J (but more slowly following a power law), so a compromise between the two is necessary.

4.3 Flux noise

Much like the charge qubit which suffers from charge noise, the decoherence of flux qubits is dominated by flux noise. Indeed, low frequency flux noise in SQUIDS has been known for a long time, with Yoshihara *et al.* (2006) first reporting $1/f$ flux noise in two flux qubits. Following Vion *et al.* (2002), the authors were able to decouple the bias current I_b from the normalised flux n_ϕ threading the qubit at optimal bias points I_b^*.

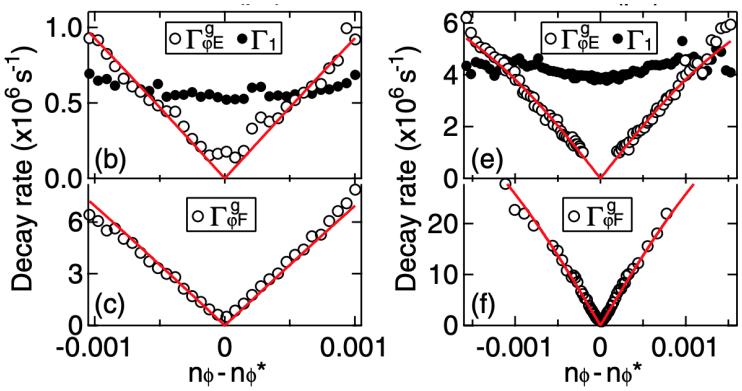

Figure 4.2. The relaxation rate Γ_1, echo pure dephasing rate $\Gamma^g_{\varphi E}$ and free induction decay pure dephasing rate $\Gamma^g_{\varphi F}$ for sample 1 (left) and sample 2 (right) as a function of the flux bias n_ϕ. A linear best fit for the dephasing rates are shown in red. Figure adapted from Yoshihara *et al.* (2006).

Operating the qubit at $I_b = I_b^*$, the decay and pure dephasing rates Γ_1 and $\Gamma^g_{\phi E}$ were measured at n_ϕ close to the optimal flux point n_ϕ^* (see fig. 4.2). A linear behaviour was observed for the pure dephasing rate in both samples, while Γ_1 was roughly constant. These results were shown to be consistent with $1/f$ flux noise, although the possible underlying physical mechanisms were not discussed at length. Similar results were also found in phase qubits by Bialczak *et al.* (2007) where the authors also found the flux noise power spectrum S_Φ to follow a $1/f^\alpha$ behaviour with $\alpha = 0.95$ and amplitude $4\mu\Phi_0/\mathrm{Hz}^{1/2}$ at 1 Hz (see fig. 4.3a). Two-level system defects were ruled out as a possible dominant source of flux noise as they would lead to flux noise approximately 4 orders of magnitude smaller.

Sendelbach *et al.* (2008) also reported a $1/f$ scaling of the flux noise in a SQUID with amplitude $3\mu\Phi_0/\mathrm{Hz}^{1/2}$ at 1 Hz, corroborating the results from Yoshihara *et al.* (2006). The authors also probed the temperature dependence of the flux noise and observed a Curie-like, paramagnetic $1/T$ scaling (see fig. 4.3b). To further analyse this temperature dependence, an external magnetic field was applied to the SQUID as it was initially cooled, and was subsequently removed in the final cooling stage at millikelvin temperatures. Through-

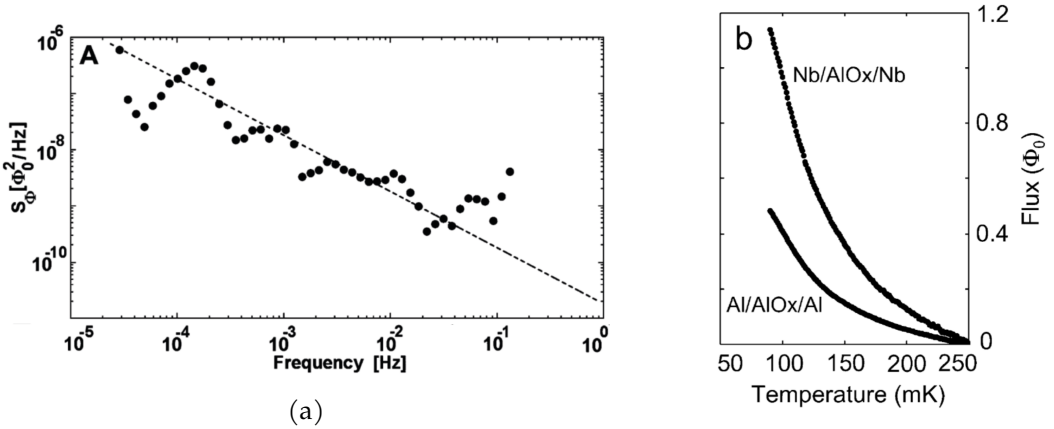

(a) (b)

Figure 4.3. (a) Flux noise power spectrum exhibiting a $1/f$ behaviour (data in dots, fit in dashed lines). Figure taken from Bialczak *et al.* (2007), (b) Temperature dependence of the quasistatic flux threading an Al SQUID and a Nb SQUID. Figure taken from Sendelbach *et al.* (2008).

out field-cool process, magnetic flux vortices get trapped on the thin film SQUID. As the temperature decreases further, the spins develop a noticeable polarisation which forces a redistribution of the magnetic flux vortices. This drives a non-zero flux through the SQUID even in the absence of applied magnetic fields (see fig. 4.4a left panel). Indeed the experimental data shows that this technique greatly enhanced the temperature dependent flux threading the SQUID, and the total flux change between 100mK and 500mK was found to grow linearly with the bias field with slope $\Delta\Phi/B_{fc} = 1.3\frac{\Phi_0}{\mathrm{mK}}$ (see fig. 4.4a right panel). These experiments established surface spins as vital to explaining flux noise in SQUIDs.

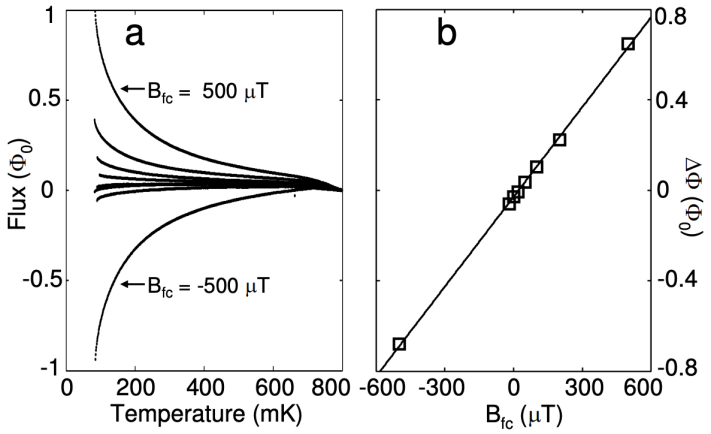

(a)

Figure 4.4. Left: Temperature-dependence of the flux threading a Nb SQUID at different applied fields. Right: the total flux change as a function of the applied field. Figures taken from Sendelbach *et al.* (2008).

Several theoretical models have been proposed to explain the origin of $1/f$ flux noise using surface spins on the SQUID thin film. One model by Wang *et al.* (2015) attributes the flux noise to adsorbed O_2 molecules on the SQUID surface interacting via a ferromagnetic XY interaction (as determined by density functional theory calculation). Using Monte Carlo simulations, the authors found a $1/f^{\alpha}$ noise spectrum with α ranging from 0.86 to 1.37, in line with experimental results. Experiments using X-ray absorption spectroscopy confirmed the presence of adsorbed O_2 molecules (Kumar *et al.* 2016). The authors of this study proposed two surface treatments to mitigate flux noise. One was to backfill the sample cell (at pressures $\sim 10^4$Pa) with NH_3 which is non-magnetic but has a higher adsorption free energy than O_2, and is therefore favoured in the surface adsorption processes of the SQUID. This technique led to a 5-fold reduction in the spectral flux noise intensity. The second treatment involved UV illumination of the sample which showed similar levels of noise reduction. Nevertheless the authors note that the treatment failed when the SQUID devices were encapsulated with SiO_x rather than SiN_x , suggesting a lower ionisation energy as the cause. Effects on flux qubit lifetimes were also not discussed.

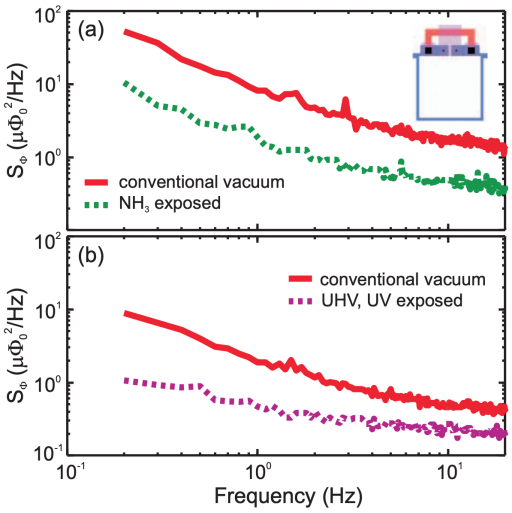

Figure 4.5. The difference in the flux noise spectrum for NH_3 exposed SQUIDs (green, top panel) and UV exposed SQUIDs (purple, bottom panel), versus at conventional conditions (red). Figure taken from Kumar *et al.* (2016).

Koch R.H., DiVincenzo and Clarke (2007) put forward a model of unpaired electrons hopping between thermally excited defects. While their obtained value of the surface spin density, $\sigma_s = 5 \times 10^{17}$, is in excellent agreement with Sendelbach *et al.* (2008), this model has a number of downsides. Firstly, it does not account for spin-spin interactions which are thought to be crucial in the dephasing dynamics. Moreover, the density of defects in oxide barriers is also too low to account for the flux noise. For instance, one should expect about 10 defects in a SQUID loop of radius 1 μm and volume 10^7nm^3 at $T = 0.1$ K, in

contrast to the $10^5 - 10^6$ defects required to match the observed noise (Faoro and Ioffe, 2008).

4.4 Dielectric losses

Most Josephson junctions are fabricated using diffusion-limited oxidation of an aluminium thin-film layer to form an amorphous oxide tunnel barrier (Oliver and Welander, 2013). However, this manufacturing process produces several defects known as two-level systems (TLSs) which can interact with electromagnetic fields via their electric dipole moments. This allows TLSs to couple to qubits causing decoherence, as was first reported by Simmonds *et al.*(2004) who detected spurious microwave resonators in phase qubits. The researchers induced $|0\rangle \rightarrow |1\rangle$ Rabi oscillations using pulsed microwaves at different bias currents. They found that the transition frequency (probed using a SQUID as detector) displayed anomalous gaps at certain bias points (top panel fig. 4.6a) which coincided with suppressed Rabi oscillation amplitudes (fig. 4.6b and bottom panel fig. 4.6a).

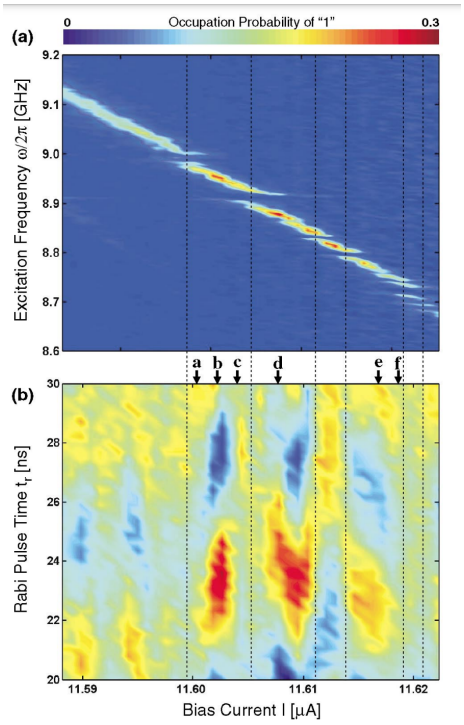

(a)

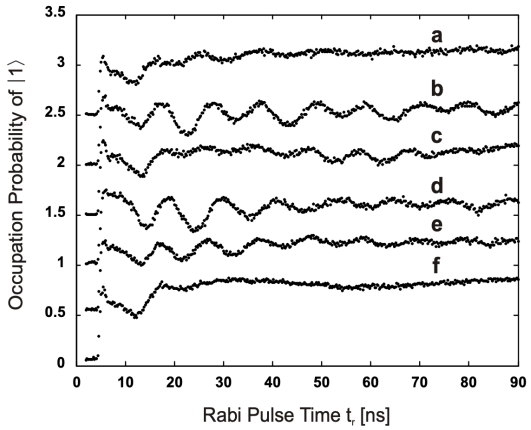

(b)

Figure 4.6. (a) Top: spectroscopy of a JJ showing spurious resonances at bias points shown with dashed lines. Bottom: $|1\rangle$ occupation probability over time as a function of the bias current. (b) Rabi oscillations (offset) at different bias currents labelled by a, b, c, d, e, f indicated with arrows in (a). Both figures taken from Simmonds *et al.* (2004).

These observations are consistent with avoided level crossings in TLSs that are resonantly

coupled to the qubit. To understand the nature of these resonators, Simmonds *et al.* (2004) propose a theoretical model of TLSs present in the aluminium oxide tunnelling barrier which couple to the qubit via fluctuations in the critical current across the JJ. The predicted critical current fluctuation was in reasonable agreement (about an order of magnitude larger) with estimates from the current-voltage characteristic of the JJ. Nevertheless, no mitigation mechanisms were proposed.

Conclusive evidence of TLS-qubit coupling was provided by Cooper *et al.* (2004). The authors introduced a novel state read-out technique in which a short bias current pulse is applied to the qubit, thus adiabatically shallowing the potential phase well and allowing $|1\rangle$ to tunnnel to neighbouring wells which can be probed using an adjacent SQUID. Because $|1\rangle$ lies near the top of the well at the peak of the bias current pulse, the tunnelling rate of $|1\rangle$ is orders of magnitude larger than $|0\rangle$ resulting in a large measurement fidelity $\eta \approx 0.96$ even for small pulse durations. Using this new technique, the researchers were able to probe the dynamics of the TLS-qubit interactions at nanosecond time scales with a resolution of 5ns. The qubit showed typical exponential decay in the tunnelling probability when tuned in the middle of the solid line in top left panel of fig. 4.7. However, when the qubit was set up near the resonance splittings, the tunnelling probability exhibited exponentially decaying oscillations. These are not Rabi oscillations as there is no driving microwave radiation (thanks to the new read-out technique). Instead the beating behaviour provides direct evidence of energy transfer between the qubit and fluctuators in the tunnelling junction. Burnett *et al.* (2019) have recently reported for the first time similar coherent qubit-TLS coupling in transmon qubits, showing that this dissipation mechanism is universal to SQubits.

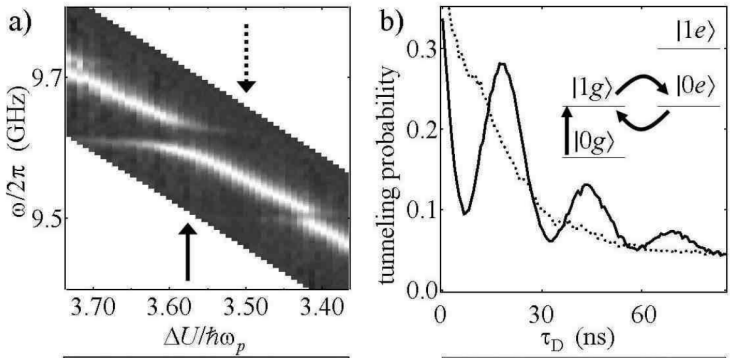

Figure 4.7. (a) Qubit spectroscopy with solid (dashed) arrow indicating on(off)-resonance. (b) Probability of tunnelling as a function of Rabi pulse time at off-resonant (dashed line) and resonant (solid line) bias currents. Both figures adapted from Cooper *et al.* (2004).

The first study to investigate the dependence of microwave resonance splittings on junction parameters was by Martinis *et al.* (2005). The researchers found that the number of

splittings decreased with the junction size, whereas the size of the resonance splittings actually increased (see section 4.4).

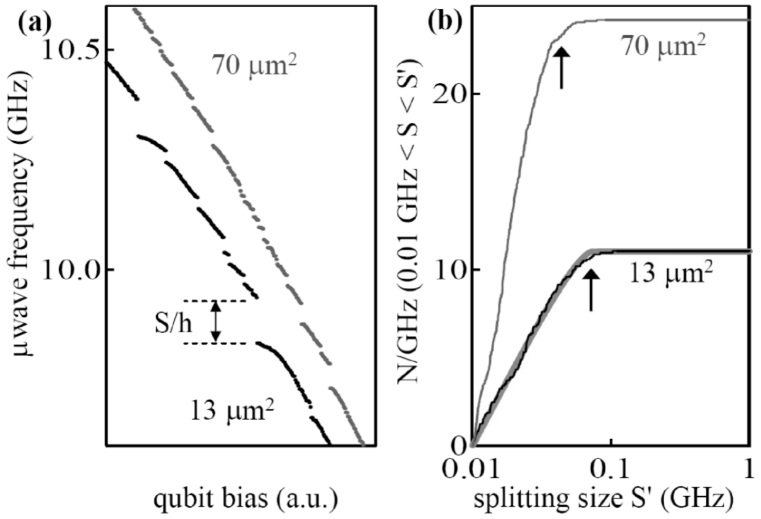

Figure 4.8. Left: spectroscopy of phase qubits with junction areas $13\mu m^2$ and $70\mu m^2$. Right: normalised cumulative distribution of the size of the resonance splittings. The solid black line shows the distribution predicted by the charge fluctuation model in the smaller qubit. Figure taken from Martinis *et al.* (2005).

In contrast to the critical-current fluctuation model proposed by Simmonds *et al.* (2004), Martinis *et al.* (2005) suggest that charge fluctuations may be behind the TLS-qubit coupling. Following this model the TLS dipole moment was estimated to be $d \approx 0.13$nm, a physically sound result which corresponds to a single charge displaced by an atomic bond in the silicon dioxide dielectric used. Furthermore, the model also yielded a prediction for the resonant frequency splitting distribution which fit the data extremely well (see section 4.4). This suggests that charge fluctuations in the TLS are the more likely/dominant candidate for dielectric loss decoherence.

CHAPTER

FIVE

DISCUSSIONS AND OUTLOOK

5.1 Approaching millisecond coherence

With groundbreaking advances in mitigating decoherence mechanisms, the operational life-times of qubits have significantly increased since the early 2000s. It is evident from fig. 5.1 that we are now entering an era of high-fidelity, millisecond coherence-time qubits. This is a tremendous breakthrough as it will soon allow SQubits to fulfill the requirements for quantum error-correction (QEC) (Barends *et al.*, 2014). Implementing QEC is fundamental to reduce errors when scaling up the number of qubits and achieve fault-tolerant computation. The philosophy behind QEC is to spread the information of a single "logical qubit" onto several, entangled "physical qubits". These physical qubits can detect and correct errors via error-correcting codes to arbitrary precision, assuming qubits have an operational error rate below a certain threshold (Kjaergaard, 2020).

Recent advances in increasing qubit coherence times came from the material sciences (Murray, 2021; Siddiqi, 2021). By changing the superconductor material from niobium to tantalum, Place *et al.* (2021) tripled T_1 from its state-of-the art value, thus reaching 0.3ms coherence times. In addition to changing the superconducting material, the researchers also upgraded the cleaning and etching processes for improved surface and edge morphology. This record was very recently extended (using the same material) to 0.5 ms by Wang *et al.* (2022) by using dry etching processes rather than wet etching. Finally, Somoroff *et al.* (2021) reported a record dephasing time of $T_2 = 1.48 \pm 0.13$ms with a gate fidelity of 0.9999 using a fluxonium qubit. However, we must emphasize that this paper has not been fully peer-reviewed nor published yet, and that there is no way for us to verify their claim.

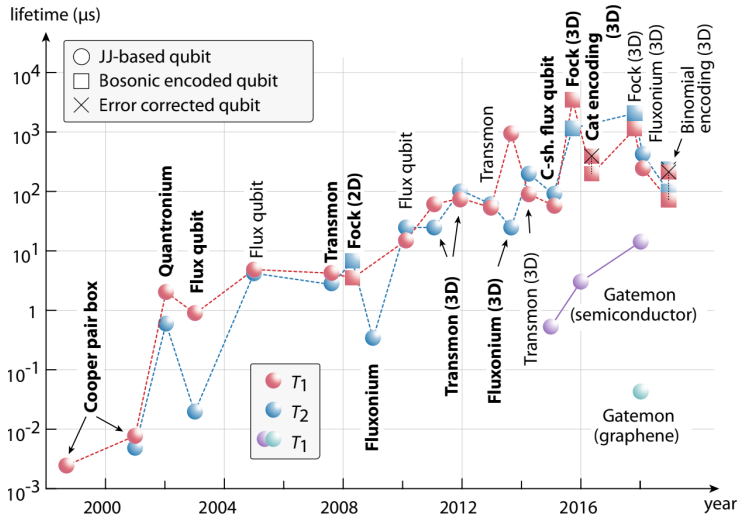

Figure 5.1. Timeline showing the progress in increasing superconducting qubit lifetimes. Figure taken from Kjaergaard (2020).

5.2 Directions for future research

Despite the immense progress that has taken place in the past 20 years, SQubits still have a long way to go before commercial implementation into quantum computers can be achieved. Here we outline some directions for future research in the decoherence of SQubits.

Firstly, as noted in chapter 4, several possible models for the sources of $1/f$ flux noise and TLS defects have been put forward in recent years, all of which have gained some level of experimental verification. Unfortunately, we are still lacking enough experimental data to reject one model over the other. In order to successfully mitigate these decoherence mechanisms, it is imperative that successful theoretical models be put forward which can rule out competing theories and obtain definitive empirical validation. In particular, while different models have presented different data as supportive evidence, we should in the future focus on relevant criteria (e.g. noise spectral intensity for $1/f$ flux noise, TLS defect density/loss tangent for dielectric losses) to benchmark these models against each other.

Furthermore, due to errors in the manufacturing process, there is currently large variability in the performance of SQubits. For example, Serniak *et al.* (2019) found that the relaxation time of transmon qubits could vary by as much as three times over a three hour period. Increasing uniformity in the manufacturing of these quantum devices will prove beneficial in the large-scale implementation of this technology.

Another aspect we have not consider thus far are the effects of multi-qubit decoherence mechanisms. More research is necessary to understand how the decoherence of single

qubits scales as they are implemented in larger and larger networks. Understanding how to diminuish interqubit cross-talk and increase control of qubit-qubit coupling by experimenting with different architectures are all crucial problems to be addressed in the future.

5.3 Milestones and predicted time-frame

In 2019, Google announced that Sycamore, their 53 qubit quantum processor using SQubits, had achieved quantum supremacy by solving a problem [1] that would require a classical computer approximately 10,000 years in just 200 seconds (Arute *et al.*, 2019). Despite this enormous milestone being achieved, we are still very far away from quantum computers capable of incorporating complex routines like Shor's algorithm. Recently the International Business Machines Corporation (IBM) announced a development roadmap for progressing quantum computing (IBM, 2022).

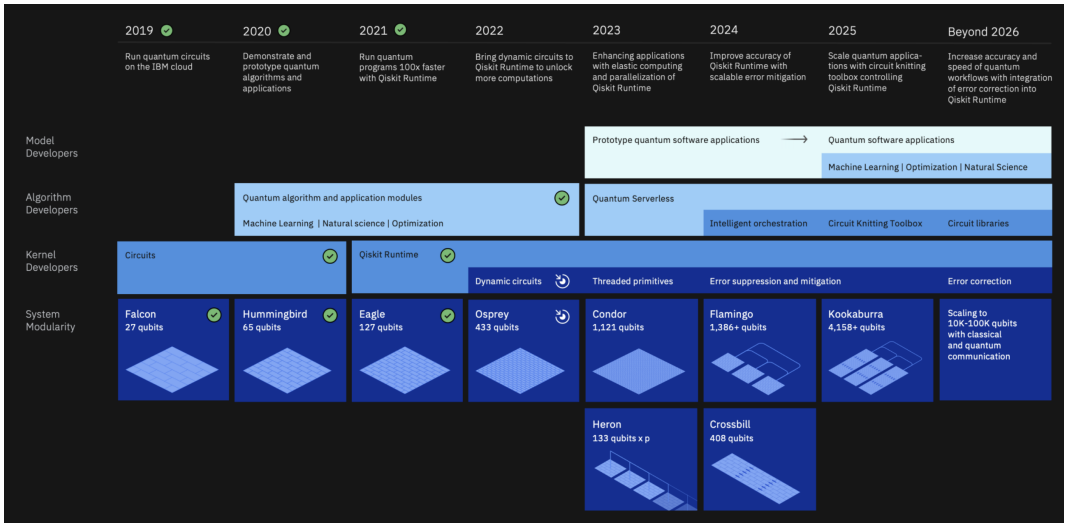

Figure 5.2. IBM's road-map for quantum computation in the near future. Figure adapted from IBM (2022).

The ambitious plan predicts a 433 qubit processor [2] by the end of this year, and estimates that 1000+ qubit processors will be introduced by 2023. As this number of qubits starts to stretch the limits of what single chip processors can do, IBM plans to produce multi-chip processors in 2024, and implement QEC in the same year.

We therefore propose the following time-frame for significant achievements in the field of superconducting quantum computing.

Milestone 1: achieving quantum supremacy with superconducting quantum qubit processor (partially achieved, 1-2 years)

[1] consisting of sampling the outputs of random circuits
[2] We note that the number of qubits is actually the number of physical qubits.

As mentioned previously, Google announced in 2019 that they had achieved quantum supremacy using their Sycamore processor. Since then, a lot of opposition to this claim has arisen, notably from IBM (who we must note is one of Google's commercial competitors) who suggested that the task Google claimed would take 10,000 years on a classical computer would realistically only take 2.5 days on their best supercomputers (Pednault *et al.*, 2019). Indeed other studies (Bulmer *et al.*, 2022; Liu et al, 2021) have confirmed that Google likely underestimated the performance of classical computers in performing the random sampling task performed by their processor. To achieve true quantum supremacy, one would need to solve a not-too-artificial problem which would take thousands of years on a classical computer. We therefore expect this milestone to be achieved in the next 1-2 years.

Milestone 2: achieve millisecond decoherence times and fidelity required for multi-qubit QEC (2-3 years)

QEC codes will be fundamental in extending the coherence lifetimes of superconducting qubit processors (Kjaergaard, 2020). However, to successfully implement these codes, individual qubits must have sufficiently long decoherence times $\sim 10^2 - 10^3 \mu$s (Rigetti *et al.*, 2012) and large enough gate fidelities $F \sim 99\%$ (Barends *et al.*, 2014) which have only been partially achieved. Extrapolating from fig. 5.1, we can expect to consistently achieve millisecond decoherence times in the next 2-3 years.

Milestone 3: quantum processor with 50 error-corrected squbits with fidelity > 99% (5-10 years)

While it has been announced that processors with 100+ SQubits, such as the Eagle processor (see fig. 5.2), have been realised, we still need to verify the quality of the qubits (most notably their coherence times and gate fidelity). It should also be noted that one error-corrected logical qubit corresponds to roughly 1000 physical qubits, so even if IBM delivers according to its roadmap, we are still far from having 50 error-corrected *logical* qubits. This would likely require new insights into the scalability of SQubits and multi-chip quantum computation. Most importantly researchers would need to understand how best to connect the quantum chips to form a single, coherent processor.

Milestone 4: quantum processor with 1000 error-corrected squbits with fidelity >99%. (10-15 years)

IBM plans to make 1000-qubit processor by 2023, but again the quality of these qubits is yet to be determined, and is unlikely to meet the criteria for error-correction to be implemented. At these scales it is expected that solutions to practical, real-word problems such as the simulation of molecules for drug discovery would start to become more feasible (Ball, 2021).

CHAPTER

SIX

CONCLUSIONS

6.1 Summary

We outlined the concepts behind the BCS theory of superconductivity and the Josephson effect. We described the properties of the three families of SQubits: charge, phase and flux qubits. We then provided a brief overview of the theory of decoherence in qubits, introducing relevant terms and notation. We subsequently identified three major sources of decoherence in SQubits: charge noise, flux noise and dielectric losses. Progress on both theoretical and experimental fronts in reducing decoherence effects were summarised, showing that while charge noise has effectively been removed via the transmon qubit design, the sources of flux noise and dielectric losses have not been fully identified yet. We compared and contrasted different competing theories regarding the sources of these decoherence channels, highlighting their strengths, weaknesses and limitations, concluding that these theoretical models are consistent with the experimental data, and can't be ruled out presently. Gaps in our knowledge of SQubit decoherence were identified and used to highlight future directions of research as we start to explore the realities of multi-qubit computation. Finally, a 10-15 year roadmap for implementations of SQubits in real quantum computers was presented.

6.2 Achievement of project objectives

The project objectives were met as follows

(i) Objective 1: chapter 2

(ii) Objective 2: chapter 3

(iii) Objective 3 chapter 4

(iv) Objective 4: chapter 5

Total word count: 4989

Acknowledgments

I would like to thank Paul Hatherly, my supervisor, for assisting me in countless ways throughout the course of this project.

REFERENCES

Bruus, H. and Flensberg, K. (2004) *Many-body quantum theory in condensed matter physics: an introduction*, New York: Oxford University Press.

Girvin, S.M. and Yang, K. (2019) *Modern condensed matter physics*. Cambridge: Cambridge University Press.

Annett, J.F. (2004) *Superconductivity, superfluids and condensates* (Vol. 5). Oxford: Oxford University Press.

Langford, N.K. (2013) *Circuit qed-lecture notes*, arXiv preprint, arXiv:1310.1897. Available at: https://arxiv.org/pdf/1310.1897.pdf (Accessed: 10 May 2022).

Simon, S. (2022) "Lecture notes for Quantum Matter". *Quantum Matter*. University of Oxford. Available at: http://www-thphys.physics.ox.ac.uk/people/SteveSimon/QCM2022/QuantumMatter.pdf(Accessed: 11 May 2022).

Girvin, S.M. (2014) "Circuit QED: superconducting qubits coupled to microwave photons". in Devoret, M., Huard, B., Schoelkopf, R. and Cugliandolo, L.F. (eds.), *Quantum machines: measurement and control of engineered quantum systems*, vol. 96. Oxford: Oxford University Press. Available at: http://www.capri-school.eu/lectureres/master_cqed_les_houches.pdf (Accessed: 12 May 2022)

Bouchiat, T., Vion D., Joyez P., Esteve D., Devoret M. H. (1998) "Quantum Coherence with a Single Cooper Pair", *Physica Scripta*, 1998(T76), p.165. Available at: https://iramis.cea.fr/spec/Pres/Quantro/Qsite/publi/articles/fichiers/preprints/98-PScripta-Bouchiat-SSbox.pdf. (Accessed: 14 May 2022)

Rigetti, C., Gambetta, J.M., Poletto, S., Plourde, B.L., Chow, J.M., Córcoles, A.D., Smolin, J.A., Merkel, S.T., Rozen, J.R., Keefe, G.A. and Rothwell, M.B. (2012) "Superconducting qubit in a waveguide cavity with a coherence time approaching 0.1 ms". *Physical Review B*, 86(10), p.100506. Available at: https://web.archive.org/web/20130409142449id_

/http://physics.syr.edu/~bplourde/papers/PRB-Rigetti12-3D-qubits-copper.pdf (Acessed: 12 March 2022)

You, J.Q. and Nori, F. (2005) "Superconducting Circuits and Quantum Information", *Physics Today*, 58(11), pp.42-47. Available at: https://qudev.phys.ethz.ch/static/content/QSIT13/pdfs/You2005.pdf (Accessed: 7 March 2022)

Yu, Y., Han, S., Chu, X., Chu, S.I. and Wang, Z. (2002) "Coherent temporal oscillations of macroscopic quantum states in a Josephson junction", *Science*, 296(5569), pp.889-892. Available at: http://wavelet.phys.ntu.edu.tw/sichu/pdf/Yu02.pdf (Accessed: 11 March 2022)

Friedman, J.R., Patel, V., Chen, W., Tolpygo, S.K. and Lukens, J.E. (2000) "Quantum superposition of distinct macroscopic states", *Nature*, 406(6791), pp.43-46. Available at: https://jrfriedman.people.amherst.edu/MacroQuantum.pdf (Accessed: 13 March 2022)

Burnett, J.J., Bengtsson, A., Scigliuzzo, M., Niepce, D., Kudra, M., Delsing, P. and Bylander, J. (2019). 'Decoherence benchmarking of superconducting qubits'. *npj Quantum Information*, 5(1), pp.1-8. Avaialble at: https://www.nature.com/articles/s41534-019-0168-5 (Accessed: 14 Mach 2022)

Nakamura, Y., Pashkin, Y.A., Yamamoto, T. and Tsai, J.S. (2002) "Charge echo in a Cooper-pair box", *Physical review letters*, 88(4), p.047901. Available at: https://arxiv.org/pdf/cond-mat/0111402.pdf (Accessed: 14 May 2022).

Devoret, M.H. and Martinis, J.M. (2004) "Implementing Qubits with Superconducting Integrated Circuits", *Quantum Information Processing*, 3(1-5). Available at: https://cpb-us-w2.wpmucdn.com/campuspress.yale.edu/dist/2/3627/files/2020/10/QIP_Devoret_squbit_review.pdf (Accessed: 19 May 2022)

Girvin, S.M. (2014) 'Circuit QED: SQubits coupled to microwave photons' in Devoret, M., Huard, B., Schoelkopf, R. and Cugliandolo, L.F. (eds.), *Quantum machines: measurement and control of engineered quantum systems*, vol. 96. Oxford: Oxford University Press. Available at: http://www.capri-school.eu/lectureres/master_cqed_les_houches.pdf (Accessed: 12 May 2022)

Vion, D., Aassime, A., Cottet, A., Joyez, P., Pothier, H., Urbina, C., Esteve, D. and Devoret, M.H. (2002) "Manipulating the quantum state of an electrical circuit", *Science*, 296(5569), pp.886-889. Available at: https://qudev.phys.ethz.ch/static/content/courses/QSIT06/pdfs/Vion02.pdf (Accessed: 6 June 2022).

Koch, J., Terri, M.Y., Gambetta, J., Houck, A.A., Schuster, D.I., Majer, J., Blais, A., Devoret, M.H., Girvin, S.M. and Schoelkopf, R.J. (2007) "Charge-insensitive qubit design derived

from the Cooper pair box", *Physical Review A*, 76(4), p.042319. Available at: https://schusterlab.stanford.edu/static/pdfs/Koch2007.pdf (Accessed: 21 May 2022).

Oliver, W.D. and Welander, P.B. (2013) "Materials in superconducting quantum bits", *MRS bulletin*, 38(10), pp.816-825. Available at: https://www.cambridge.org/core/journals/mrs-bulletin/article/materials-in-superconducting-quantum-bits/B7A4DC8B7F54A0715CEFAFE6677F33D8 (Accessed: 21 May 2022).

Martinis, J.M., Cooper, K.B., McDermott, R., Steffen, M., Ansmann, M., Osborn, K.D., Cicak, K., Oh, S., Pappas, D.P., Simmonds, R.W. and Clare, C.Y. (2005) "Decoherence in Josephson qubits from dielectric loss", *Physical review letters*, 95(21), p.210503. Available at: http://web.physics.ucsb.edu/~martinisgroup/papers/Martinis2005.pdf (Accessed: 25 May 2022).

Simmonds, R.W., Lang, K.M., Hite, D.A., Nam, S., Pappas, D.P. and Martinis, J.M. (2004) "Decoherence in Josephson phase qubits from junction resonators", *Physical Review Letters*, 93(7), p.077003. Available at: http://web.physics.ucsb.edu/~martinisgroup/papers/Simmonds2004b.pdf (Accessed: 25 May 2022).

Cooper, K.B., Steffen, M., McDermott, R., Simmonds, R.W., Oh, S., Hite, D.A., Pappas, D.P. and Martinis, J.M. (2004) "Observation of quantum oscillations between a Josephson phase qubit and a microscopic resonator using fast readout", *Physical Review Letters*, 93(18), p.180401. Available at https://web.physics.ucsb.edu/~martinisgroup/papers/0405710.pdf (Accessed: 28 May 2022).

Yoshihara, F., Harrabi, K., Niskanen, A.O., Nakamura, Y. and Tsai, J.S. (2006) "Decoherence of flux qubits due to 1/f flux noise", *Physical review letters*, 97(16), p.167001. Available at: https://web.archive.org/web/20190217225148id_/http://pdfs.semanticscholar.org/08cf/661f9e1a8659e0a7bc9d38e337fa778389e9.pdf (Accessed: 28 May 2022).

Bialczak, R.C., McDermott, R., Ansmann, M., Hofheinz, M., Katz, N., Lucero, E., Neeley, M., O'Connell, A.D., Wang, H., Cleland, A.N. and Martinis, J.M. (2007) "1/f flux noise in Josephson phase qubits", *Physical review letters*, 99(18), p.187006. Available at: https://web.physics.ucsb.edu/~martinisgroup/papers/Bialczak2007.pdf (Accessed: 1 June 2022).

Sendelbach, S., Hover, D., Kittel, A., Mück, M., Martinis, J.M. and McDermott, R. (2008) "Magnetism in SQUIDs at millikelvin temperatures", *Physical review letters*, 100(22), p.227006. Available at: https://uol.de/f/5/inst/physik/ag/monet/Publikationen/Magnetism_in_SQUIDs_at_Millikelvin_Temperatures.pdf (Accessed: 1 June 2022).

Wang, H., Shi, C., Hu, J., Han, S., Clare, C.Y. and Wu, R.Q. (2015) "Candidate source of

flux noise in SQUIDs: adsorbed oxygen molecules", *Physical review letters*, 115(7), p.077002. Available at: https://ps.uci.edu/~cyu/publications/PRLWangDFT_O2FluxNoise2015.pdf (Accessed: 3 June 2022).

Kumar, P., Sendelbach, S., Beck, M.A., Freeland, J.W., Wang, Z., Wang, H., Clare, C.Y., Wu, R.Q., Pappas, D.P. and McDermott, R. (2016) "Origin and reduction of 1/f magnetic flux noise in superconducting devices", *Physical Review Applied*, 6(4), p.041001. https://ps.uci.edu/~cyu/publications/PRApp_XMCD_2016.pdf (Accessed: 3 June 2022).

Koch, R.H., DiVincenzo, D.P. and Clarke, J. (2007) "Model for 1/f flux noise in SQUIDs and qubits", *Physical review letters*, 98(26), p.267003. Available at: https://core.ac.uk/download/pdf/71305445.pdf (Accessed: 6 June 2022).

Faoro, L. and Ioffe, L.B. (2008) "Microscopic origin of low-frequency flux noise in Josephson circuits", *Physical review letters*, 100(22), p.227005. Available at: https://arxiv.org/pdf/0712.2834.pdf. (Accessed: 6 June 2022).

Schlosshauer, M. (2019) "Quantum decoherence", *Physics Reports*, 831, pp.1-57. Available at: http://faculty.up.edu/schlosshauer/publications/Schlosshauer_QuantumDecoherence_PhysRep.pdf. (Accessed: 9 June 2022).

Kjaergaard, M., Schwartz, M.E., Braumüller, J., Krantz, P., Wang, J.I.J., Gustavsson, S. and Oliver, W.D. (2020) "SQubits: Current State of Play", *Annual Review of Condensed Matter Physics*, 11, pp.369-395. Available at: https://arxiv.org/pdf/1905.13641.pdf (Accessed: 10 June 2022).

Barends, R., Kelly, J., Megrant, A., Veitia, A., Sank, D., Jeffrey, E., White, T.C., Mutus, J., Fowler, A.G., Campbell, B. and Chen, Y. (2014) "Superconducting quantum circuits at the surface code threshold for fault tolerance", *Nature*, 508(7497), pp.500-503. Available at: https://clelandlab.uchicago.edu/pdf/barends%20benchmark%20nature%202014.pdf (Accessed: 10 June 2022).

Murray, C.E. (2021) "Material matters in SQubits", *Materials Science and Engineering: R: Reports*, 146, p.100646. Available at https://arxiv.org/pdf/2106.05919.pdf (Accessed: 12 June 2022).

Siddiqi, I. (2021) "Engineering high-coherence SQubits", *Nature Reviews Materials*, 6(10), pp.875-891. Available at: https://escholarship.org/content/qt46523263/qt46523263_noSplash_158a0df86d215bd799a14595fe120c02.pdf (Accessed: 12 June 2022).

Place, A.P., Rodgers, L.V., Mundada, P., Smitham, B.M., Fitzpatrick, M., Leng, Z., Premkumar, A., Bryon, J., Vrajitoarea, A., Sussman, S. and Cheng, G. (2021) "New material platform for superconducting transmon qubits with coherence times exceeding 0.3 millisec-

onds", *Nature communications*, 12(1), pp.1-6. Available at: https://www.nature.com/articles/s41467-021-22030-5.pdf (Accessed: 16 June 2022).

Wang, C., Li, X., Xu, H., Li, Z., Wang, J., Yang, Z., Mi, Z., Liang, X., Su, T., Yang, C. and Wang, G. (2022) "Towards practical quantum computers: transmon qubit with a lifetime approaching 0.5 milliseconds", *npj Quantum Information*, 8(1), pp.1-6. Available at: https://www.nature.com/articles/s41534-021-00510-2.pdf (Accessed: 18 June 2022).

Somoroff, A., Ficheux, Q., Mencia, R.A., Xiong, H., Kuzmin, R.V. and Manucharyan, V.E. (2021) "Millisecond coherence in a superconducting qubit", *arXiv preprint*, arXiv:2103.08578. Available at: https://arxiv.org/pdf/2103.08578.pdf (Accessed: 19 June 2022).

Serniak, K., Diamond, S., Hays, M., Fatemi, V., Shankar, S., Frunzio, L., Schoelkopf, R.J. and Devoret, M.H. (2019) "Direct dispersive monitoring of charge parity in offset-charge-sensitive transmons", *Physical Review Applied*, 12(1), p.014052. Available at: https://rsl.yale.edu/sites/default/files/2019-serniak-direct_dispersive_monitoring_of_charge_parity_in_offset-charge-sensitive_transmons_0.pdf (Accessed: 18 July 2022).

Arute, F., Arya, K., Babbush, R., Bacon, D., Bardin, J.C., Barends, R., Biswas, R., Boixo, S., Brandao, F.G., Buell, D.A. and Burkett, B. (2019) "Quantum supremacy using a programmable superconducting processor", *Nature*, 574(7779), pp.505-510. Available at: https://www-nature-com.libezproxy.open.ac.uk/articles/s41586-019-1666-5.pdf (Accessed: 4 August 2022).

International Business Machines Corporation. (2022) *Our new 2022 Development Roadmap*. Available at: https://www.ibm.com/quantum/roadmap (Accessed: 7 August 2022).

Bulmer, J.F., Bell, B.A., Chadwick, R.S., Jones, A.E., Moise, D., Rigazzi, A., Thorbecke, J., Haus, U.U., Van Vaerenbergh, T., Patel, R.B. and Walmsley, I.A. (2022) "The boundary for quantum advantage in Gaussian boson sampling". *Science advances*, 8(4), p.eabl9236. Available at: https://www.science.org/doi/full/10.1126/sciadv.abl9236?fbclid=IwAR0mjCIA15tj5ZX1SnlFRBb6W93GjlRJOMF_KUGfY5ZBwFa5X0pXiMooxJ0&intcmp=trendmd-adv&adobe_mc=MCMID%3D32100606165266186296740783268588076688%7CMCORGID%3D242B6472541199F70A4C98A6%2540AdobeOrg%7CTS%3D1650153600 (Accessed: 8 August 2022).

Liu, Y., Liu, X., Li, F., Fu, H., Yang, Y., Song, J., Zhao, P., Wang, Z., Peng, D., Chen, H. and Guo, C. (2021) "Closing the" quantum supremacy" gap: achieving real-time simulation of a random quantum circuit using a new sunway supercomputer". *In Proceedings of the International Conference for High Performance Computing, Networking, Storage and Analysis*, pp.

1-12. Available at: https://dl.acm.org/doi/pdf/10.1145/3458817.3487399 (Accessed: 8 August 2022).

Pednault, E., Gunnels, J., Maslov, D., Gambetta, J. (2019) *On "Quantum supermacy"*. Available at: https://www.ibm.com/blogs/research/2019/10/on-quantum-supremacy/ (Accessed: 12 August 2022).

Ball, P. (2021) "First quantum computer to pack 100 qubits enters crowded race", *Nature*, 599(7886), pp.542-542. Available at: https://media.nature.com/original/magazine-assets/d41586-021-03476-5/d41586-021-03476-5.pdf (Accessed: 16 August 2022).